Published in final edited form as:
Nat Cell Biol. 2017 June ; 19(6): 639–652. doi:10.1038/ncb3534.

Endoglin prevents vascular malformation by regulating flow-induced cell migration and specification through VEGFR2 signalling

Yi Jin[1], **Lars Muhl**[1], **Mikhail Burmakin**[1], **Yixin Wang**[1], **Anne-Claire Duchez**[1], **Christer Betsholtz**[2,3], **Helen M. Arthur**[4], and **Lars Jakobsson**[1]

[1]Dept. of Medical Biochemistry and Biophysics, Karolinska Institutet, Scheeles väg 2, 171 77 Stockholm, Sweden

[2]Dept. of Immunology, Genetics and Pathology, Uppsala University, Uppsala, Sweden

[3]Integrated Cardio Metabolic Centre (ICMC), Karolinska Institutet, Novum, Blickagången 6, SE14157 Huddinge, Sweden

[4]Institute of Genetic Medicine, International Centre for Life, Newcastle University, Newcastle upon Tyne, NE1 3BZ, UK

Abstract

Loss-of-function (LOF) mutations in the endothelial cell (EC) enriched gene endoglin (*ENG)* causes the human disease hereditary haemorrhagic telangiectasia-1, characterized by vascular malformations promoted by vascular endothelial growth factor A (VEGFA). How ENG deficiency alters EC behaviour to trigger these anomalies is not understood. Mosaic ENG deletion in the postnatal mouse rendered *Eng* LOF ECs insensitive to flow-mediated venous to arterial migration. *Eng* LOF ECs retained within arterioles acquired venous characteristics and secondary ENG-independent proliferation resulting in arterio-venous malformation (AVM). Analysis following simultaneous *Eng* LOF and overexpression (OE) revealed that *ENG* OE ECs dominate tip cell positions and home preferentially to arteries. *ENG* knock-down altered VEGFA-mediated VEGFR2 kinetics and promoted AKT signalling. Blockage of PI3K/AKT partly normalised flow-directed migration of *ENG* LOF ECs in vitro and reduced the severity of AVM in vivo. This demonstrates the requirement of ENG in flow-mediated migration and modulation of VEGFR2 signalling in vascular patterning.

Correspondence should be addressed to: Lars Jakobsson, Division of Vascular Biology, Department of Medical Biochemistry and Biophysics, Karolinska Institutet, Scheeles väg 2, Stockholm, Sweden, Lars.Jakobsson@ki.se.

Author contribution

L.J., Y.J. and L.M. designed the research; Y.J., L.M., C.B., H.M.A., and L.J. wrote the paper; Y.J., L.M., Y.W., M.B. and A.C.D. performed the experiments and together with L.J. analysed the data. All authors discussed the results and commented on the manuscript.

Competing Financial Interests

The authors declare no competing financial interests.

Europe PMC Funders Author Manuscripts

Development of the blood vasculature into a hierarchical network of arteries, capillaries and veins involves tip cell selection, migration, proliferation, mural cell recruitment, fusion of sprouts (anastomosis), lumen formation, growth and pruning1. These vessel rearrangements rely on a precise coordinated behaviour of individual ECs to gain and sustain hierarchy and functionality, controlled by cell signalling and flow-mediated shear forces2. The initiation and formation of new branches, known as sprouting angiogenesis, is driven by VEGFA3 and fine-tuned via the Jagged/Delta-like/Notch cascades4–9. Interference with these systems results in vessel patterning defects9–13. One such defect is manifested by direct shunts between arteries and veins, so called arterio-venous malformations (AVMs). LOF mutations in either *ENG* or *ACVRL1* (*Activin receptor like kinase 1,* also known as *ALK1*) cause the human vascular diseases hereditary haemorrhagic telangiectasia (HHT) -1 and -2, respectively. HHT, also known as Osler Weber Rendu Syndrome, is characterized by vessel patterning defects causing micro-aneurysms (telangiectases) with bleedings in skin and mucosal membranes, as well as AVMs in brain, lung and liver. Whether mechanisms of tip-stalk cell selection, EC migration and proliferation are intimately connected with AVM development remains to be determined.

Postnatal conditional EC-specific deletion of *Eng* or *Alk1* in the mouse leads to development of AVMs, and represents valuable models of HHT. However, while *Eng* LOF has a mild hyperbranching phenotype *Alk1* LOF strongly promotes tip cell potential as well as branching14–16. ENG and ALK1 are receptors involved in the transforming growth factor beta (TGFβ)/Bone morphogenetic protein (BMP) pathway mediating downstream activation of the SMAD1/5/8 transcription factors17, that modulate vascular patterning18.

Observations in HHT1 patients and in genetic mouse models with *ENG* LOF mutations indicate that AVMs are triggered by wounding and/or by VEGFA administration19–22. Recent clinical trials utilizing VEGFA inhibition for treatment of HHT have highlighted the impact of VEGFA on promoting the establishment of AVMs23, 24. Despite these findings the functional link between VEGF and ENG remains unknown. Also, how *Eng* deletion transmits into altered cellular behaviour resulting in AVM has been unresolved, as has the potential arterial/capillary/venous preference for AVM initiation. Here we describe the impact of *Eng* LOF on cellular behaviour in sprouting angiogenesis, vascular remodelling and AVM, involving an ENG-mediated modulation of VEGFR2 signalling. We conclude that ENG cell-autonomously controls EC migration during vessel remodelling in response to VEGFA and shear stress; a process that is required for the establishment of arterio-venous vessel hierarchy. In *Eng* LOF mice, ECs fail to establish arteriole-properties and instead acquire venous characteristics with secondary proliferation and expansion leading to AVM. Hence arterioles are the main initial sites of malformation. In addition, our data functionally uncouple the processes of enhanced sprouting angiogenesis and AVM in HHT.

Results

Postnatal EC-specific deletion of *Eng* causes local unique phenotypes: -Primary AVM and secondary hypersprouting

Here we demonstrate that tamoxifen-induced EC-specific deletion of *Eng* at postnatal day (P) 1 in $Eng^{flox/flox}$:$Cdh5(PAC)CreER^{T2}$:*R26Ryfp* (hence forth denoted $Eng^{i\Delta EC}$) mice leads

to local AVMs within the cerebral vasculature at P7 and at the same time promotes sprouting angiogenesis as indicated by the increase in angiogenic tip cells (Fig. 1a-c). Immunostaining revealed that the vast majority of YFP positive cells had lost expression of ENG protein (Supplementary Fig. 1a), confirming that conditional expression of YFP serves as a reliable marker for *Eng* deletion. *Vegfa* transcripts were 2.3 fold higher in whole brain lysates from *Eng* LOF pups compared to littermate controls, indicating reduced oxygen supply (Fig. 1d). In accordance with previous studies, the retinal vasculature of *Eng* LOF mice displayed AVMs and reduced radial expansion14 (Fig. 1e). In retinas with large AVMs, areas with excessive sprouting correlated with local hypoxic regions as indicated by pimonidazole staining (Supplementary Fig. 1b). Also, deletion of *Eng* at P4 and analysis of P7 retinas revealed that local *Eng* deletion is insufficient to induce excessive sprouting and reduction in radial expansion, and that these phenomena rely on the presence of AVMs (Fig. 1e). Furthermore, sporadic microvascular/glomeruloid tufts, composed of wildtype (WT) cells only appeared within the brain vasculature of *Eng* LOF mice when induced at P1 (Supplementary Fig. 1c). These findings suggest that enhanced sprouting as well as tuft formation are secondary to AVM and likely caused by a hypoxia-induced increase in VEGFA as a consequence of reduced vascular functionality.

Loss of *Eng* cell-autonomously suppresses tip cell potential in competition with WT or *ENG* overexpressing ECs

To further investigate ENG's role in vascular morphogenesis we characterized its expression within the postnatal brain and retinal vasculature, where *Eng* was specific and abundant within the endothelium but strongly reduced in tip cells compared to stalk cells (Fig. 2a-c). This was confirmed by *Eng-lacZ* reporter activity in $Eng^{lacZ/wt}$ mice at P7 (Supplementary Fig. 2a, b), establishing *Eng* as a stalk cell-enriched gene. In addition *Eng* expression was high in veins and arterioles but low in major arteries at P7 (Supplementary Fig. 2b). In adults the expression was further potentiated in ECs of arterioles that branch from the main arteries (Supplementary Fig. 2c).

The distinct differential tip-stalk expression of *Eng* in vivo suggested a role in tip-stalk selection, analogous to that of the ALK1 receptor16, 25, 26. To investigate this possibility, $Eng^{i\Delta EC}$ mice were treated with low dose tamoxifen at P1 to induce cellular mosaicism for *Eng* deletion. Clonal analysis of *Eng* LOF cells in the mosaic sprouting vasculature of retinas at P7 revealed that they were under-represented in the sprouting front (Fig. 2d, e). Similar distribution was evident in the developing cerebral vasculature, where 60% of the tip cells were WT (YFP-) and 40% *Eng* LOF cells (YFP+) in $Eng^{i\Delta EC}$ mice compared to 51% (YFP-)/ 49% (YFP+) cells in control mice (Fig. 2f, g). To uncouple the endogenous regulation of *Eng*, a transgenic mouse with conditional overexpression (OE) of human *ENG* (h*ENG*, the mouse denoted Eng^{iECOE})27 was crossed with $Eng^{i\Delta EC}$ mice to generate $Eng^{i\Delta EC+iOE}$. Due to different recombination efficiency of LOF and OE alleles, mosaic *ENG* OE could be studied in the background of complete *Eng* deletion (Supplementary Fig. 3a). In these mice, h*ENG* OE cells were clearly overrepresented within the tip cell population compared with *Eng* LOF cells in retina (86% vs. 14%, Fig. 2h, i) as well as cerebrum (Fig. 2j, k). These data suggest that ENG can act in a cell autonomous manner to promote tip cell competence. Down-regulation of *Eng* in tip cells in the WT situation may hence function to

limit sprout elongation and to facilitate anastomosis. To acquire transcriptional information from *Eng* LOF and WT cells within the same vasculature, a mouse with endothelial specific GFP expression (Claudin5-GFP, Supplementary Fig. 3b) was crossed with $Eng^{flox/flox}$ mice carrying a conditional nuclear localised fluorophore (R26R-H2B-mCherry). Comparison between sorted *Eng* LOF ECs and WT ECs from mosaic brains of the same mice (Fig. 2l) revealed no difference in the tip-cell enriched genes *Dll4* and *Cxcr4* (Fig. 2m). However *Id1, Hey1* and *Ephrinb2,* were downregulated in *Eng* LOF ECs, suggesting a shift towards a more venous identity (Fig. 2m). These data confirm cell-autonomous effects of *Eng* deletion and show that ENG and ALK1 function in opposite ways in regulating sprouting angiogenesis, despite similar AVM phenotypes following *Eng* and *ALK1* LOF16, 25. Taken together this suggests that sprouting angiogenesis and AVM in HHT result from different mechanisms and that these biological phenomena are not functionally linked.

Eng LOF ECs in angiogenic sprouts ex vivo display reduced migratory capacity

To elucidate the impact of ENG on EC behaviour and VEGFA-driven EC responses in the absence of potential systemic effects, we studied sprouting angiogenesis in aortic explant cultures with or without VEGFA (Fig. 3a), utilizing time-lapse microscopy. EC tracking was facilitated by an endogenous conditional nuclear localised fluorophore in either control or *Eng* LOF mice ($Eng^{wt/wt}$:*Cdh5(PAC)CreER*^{T2}:*R26R-H2B-mCherry* or $Eng^{flox/flox}$:*Cdh5(PAC)CreER*^{T2} :*R26R-H2B-mCherry*), (Supplementary Fig. 4). Following recombination, EC nuclei were tracked by fluorescence microscopy (Fig. 3b, Supplementary video 1). There was no effect on sprout elongation but an increase in sprout diameter in *Eng* LOF cultures (Fig. 3c, d). In addition *Eng* LOF ECs showed reduced migration velocity, compared to controls, both with and without VEGFA (Fig. 3e). Nevertheless VEGFA significantly increased sprout elongation and migration speed of *Eng* LOF ECs (Fig. 3c, e). During angiogenesis, ECs migrate towards the tip (anterograde), stay still, or move away from the tip (retrograde)26, 28. Here, VEGFA treatment promoted anterograde migration of both WT and *Eng* LOF ECs (Fig. 3f, g). Also, *Eng* LOF ECs stayed still for a longer time than WT cells (Fig. 3h).

Taken together, the data indicate that VEGFA promotes migration and sprouting of ECs, in a partly ENG dependent manner, in support of the idea that ENG promotes angiogenesis cell-autonomously (Fig. 3e-g).

AVM expansion, but not initiation, involves *Eng* LOF-mediated proliferation

The retinal vasculature of *Eng* LOF mice has been reported to be hyper proliferative, but information on spatial differences, potential cell-autonomous effects, and involvement in AVM formation is missing14. To investigate this, we induced mosaic *Eng* deletion at P1, utilising conditional nuclear- mCherry expression to identify recombined ECs. EdU (5-ethynyl-2-deoxyuridine) injection at P7, and co-staining for the EC-specific transcription factor ERG1 revealed an increase in proliferation of *Eng* LOF cells compared to WT cells in mosaic but phenotypically normal vessels (non-AVM) of the brain (Fig. 4a, b and d). In mosaic AVM-like structures *Eng* LOF EC proliferation was further increased, here accompanied by increased WT cell proliferation (Fig. 4c, d). Note that in these brains VEGFA was increased (Fig. 1d). A similar analysis was performed in retinas in which

arteries, veins and capillaries could be identified based on morphological criteria. With low degree of recombination and no AVMs, proliferation was similar between *Eng* LOF and non-recombined ECs and also not different from ECs in control retinas (Fig. 4e). However, in retinas with a higher recombination rate and with AVMs, *Eng* LOF ECs showed a higher degree of proliferation compared to non-recombined ECs, in vessels outside of the AVMs (Fig. 4e). Within AVMs both cell populations displayed an equal increase in proliferation (Fig. 4e). We then analysed general proliferation of retinal ECs specifically in arteries, veins, capillaries and found no change in proliferation in retinas lacking AVMs (Fig. 4f, g). In retinas with AVM however, proliferation was specifically increased in arteries as well as in AVMs.

Altogether these analyses indicate that ENG is not a major player in regulation of proliferation in normal development, or during the initiation of AVM, but that *Eng* deletion promotes cell-autonomous proliferation upon disturbed vessel function, potentially relating to increased VEGFA levels. The equal increase in proliferation of *Eng* LOF and WT ECs in mosaic retinal AVMs, indicates however that AVM expansion involves additional mechanisms to those directly induced by *Eng* deletion.

Eng deletion disrupts arterio-venous EC distribution causing arteriole-derived AVM

To elucidate ENG's importance for vascular patterning, remodelling and potential role in migration in vivo, we induced mosaic EC-specific deletion of *Eng* and analysed the localisation of recombined YFP-positive cells in the retinal vasculature. In control mice, carrying the conditional YFP reporter, recombined cells distributed evenly throughout the vasculature 6 days post recombination (Fig. 5a, b). In mosaic $Eng^{i\Delta EC}$ mice however, recombined ECs (*Eng* LOF) were found enriched in the main veins compared to "near-venous" regions, arteries and "near-artery" regions (Fig. 5c, d). In contrast, following mosaic recombination in Eng^{iECOE} mice, *Eng* OE cells showed preferential location to arteries (Fig. 5e, f). To investigate the impact of differential ENG expression on arterio-venous sorting, we analysed cellular distribution of h*ENG* OE cells in the background of complete *Eng* deletion using the $Eng^{i\Delta EC+iOE}$ mice. In this scenario, veins and AVMs were devoid of h*ENG* OE cells, which accumulated in arteries (Fig. 5g, h). Only in the case of near complete induction of h*ENG* overexpression in $Eng^{i\Delta EC+iOE}$ mice, the AVM phenotype was rescued (Supplementary Fig. 5a). Together these experiments designate ENG as a key protein balancing the distribution of ECs to the arterial or venous regions within the developing vasculature.

To determine the anatomical origin of AVMs, mosaic *Eng* deletion ($Eng^{i\Delta EC}$) was induced at P4 and the retinal vasculature analysed at P7. Three days following deletion, arterioles with high recombination were frequently enlarged suggestive of AVM initiation (Fig. 5i). After six days malformations were more frequent and pronounced within arterioles, displaying accumulation of recombined cells (Fig. 5i, j). To investigate the successive development of AVMs from the early arteriole-specific malformations, $Eng^{i\Delta EC}$ mice were induced at P4 and analysed at P6, 7, 8 and 10. These analyses suggest that enlarged arterioles gradually expand to the adjacent veins to establish the AV shunts (Supplementary Fig. 5b). AVMs acquired venous characteristics as indicated by the venous-typical pattern of smooth muscle

cell coverage and reduced DLL4 expression (Supplementary Fig. 5b, c). These data provide evidence for an arteriolar origin of ENG-related AVMs, which are primarily initialised by regional accumulation of *Eng* LOF cells possibly as a consequence of their reduced ability of migrating against the direction of flow. However, clonal analysis of the mosaic retinal vasculature of $Eng^{flox/flox}$:*Cdh5(PAC)CreER*^{T2} :*R26R-H2B-mCherry* mice, revealed an equal relative contribution of WT and *Eng* LOF ECs (mCherry+) to established AVMs and the complete vasculature (Fig. 5k, l), suggesting non-cell autonomous mechanisms contributing to the expansion of AVMs.

ENG promotes flow-mediated directional up-stream migration of ECs

During vascular development ECs have been reported to polarize and migrate in a manner dependent on flow direction and magnitude2, 26, 29–32. It has also been shown that arteries are formed by migration of ECs from veins30. The specific localisation of *Eng* LOF and *Eng* OE ECs in the mosaic retinal vasculature may relate to alterations in flow-mediated migration. To this end, fully confluent WT or *ENG* knockdown (lentiviral-mediated shRNA) human dermal microvascular endothelial cells (HDMECs), were subjected to laminar flow and imaged by time-lapse microscopy (Fig. 6a, Supplementary videos 2, 3). Tracking of cell migration showed no difference in overall migratory distance (Fig 6b). Whereas the majority of control cells moved against flow, the majority of *ENG* knockdown cells instead migrated with the flow (Fig. 6c, d). Isolated lung ECs from P7 $Eng^{i\Delta EC}$ and control mice recapitulated this behaviour. In addition, ENG OE ECs from Eng^{iECOE} mice showed enhanced migration against flow, altogether indicating that ENG promotes flow-regulated migration in a dose-dependent manner (Fig. 6e). The effects were not due to major alterations in classical shear stress regulated genes as WT and ENG knockdown ECs responded to shear stress by the expected up-regulation of *KLF2* and *JAG1* (Fig. 6f-h). However *HEY1* was down-regulated by flow in control cells but not in *ENG* knockdown cells, in which *HEY1* was already lower in the no-flow state (Fig. 6i). To investigate whether *Eng* LOF may affect flow-induced polarisation in vivo, positioning of the Golgi apparatuses relative to their respective nuclei and flow direction was analysed in arterioles of postnatal retinas. As expected ECs of WT mice regularly polarized against flow direction32 (Supplementary Fig. 6a, d). However with mosaic *Eng* LOF, the fraction of cells showing altered polarisation was increased within *Eng* LOF cells compared to WT (Supplementary Fig. 6b, e). In AVMs, both WT and LOF cells were abnormally polarized (Supplementary Fig. 6c, f), again suggesting a non-cell autonomous effect during growth of established AVMs.

To study the effect of ENG on flow-regulated migration in vivo, we performed in vivo imaging to track individual ECs within remodelling vessels of wounded corneae of $Eng^{i\Delta EC}$ and control mice. Induced YFP expression (mosaic recombination) permitted identification and tracking of individual ECs (Fig. 6j, Supplementary video 4). Out of the trackable motile ECs in control mice 72% migrated towards the flow direction, compared to only 39% in *Eng* LOF mice (Fig. 6k, l).

ENG deletion alters VEGFA-induced VEGFR2 kinetics and downstream signalling

A line of in vivo experimental data indicates that the establishment of AVMs in adult *Eng* heterozygote or *Eng* LOF mice is triggered by the presence of VEGFA19, 20. In spite of

this, no obvious differences in VEGFR2 phosphorylation or its downstream signalling components have been reported33. To investigate this, ENG was downregulated in HDMECs by lentiviral transduction of shRNA (sh*ENG*). *ENG* knockdown did not alter the magnitude or kinetics of VEGFA-induced tyrosine phosphorylation of VEGFR2 (Fig. 7a, b). However, *ENG* knockdown cells exhibited a reduced time-dependent decrease of total VEGFR2 following VEGFA stimulation compared to control (Fig. 7c, d). In addition sh*ENG* ECs displayed enhanced activation of the VEGFR2 down-stream kinase AKT while ERK1/2 activation was not affected (Fig. 7e-g). This suggests a differential activation of VEGFR2 downstream pathways, dependent on ENG.

To specifically study VEGFR2 at the plasma membrane (i.e. glycosylated VEGFR2) the membrane protein fraction was isolated utilizing cell surface biotinylation. VEGFA treatment induced a gradual clearance of VEGFR2 from the membrane in control and sh*ENG* ECs but the latter displayed a slightly altered VEGFR2 internalisation kinetics. Whereas VEGFR2 continued to decrease from 30-60 minutes in the WT, no further reduction was seen in ENG knockdown cells (Fig. 7h, i), suggesting an increased recycling of VEGFR2 to the plasma membrane in sh*ENG* ECs. No significant difference in phosphorylation of membrane-located VEGFR2 was observed, in line with our data from whole cell lysates (Fig. 7h, j). Furthermore, immunostaining for VEGFR2 and ENG showed co-localisation in subsets of cytoplasmic vesicles of VEGFA treated HDMECs (Fig 7k) as well as in ECs of P7 mouse brains (Supplementary Fig. 7a). Co-localisation of VEGFR2 and ENG were frequently found in EEA1, Rab5 or Rab7 positive endosomes while rarely in endoplasmic reticulum, suggesting potential physical interaction between VEGFR2 and ENG, at least during intracellular trafficking and endosomal sorting (Supplementary Fig. 7b). However, to resolve the precise role of ENG on VEGFR2 trafficking would require further investigation.

Inhibition of VEGFR2 or PI3K signalling reduces the severity of *Eng* LOF-mediated AVM

To test the relevance of altered VEGFR2 activity and downstream signalling on the development of AVM in vivo, the VEGFR2 kinase inhibitor, SU5416, or the phosphoinositide 3-kinases (PI3K)-AKT inhibitor Wortmannin were administered daily (P4-6) to *Eng* LOF pups (LOF induced at P3). Both treatments tended to reduce the frequency of AVMs in *Eng* LOF pups and significantly reduced the severity of the AVMs as indicated by less distorted vascular morphology and smaller diameters of the AV shunts in P7 retinas (Fig. 8a, b, c). To investigate the respective drugs' effects on flow-mediated cell behaviour, ECs exposed to flow were treated and live-imaged as described above (Fig. 6a). The general migration speed of both control and *ENG* knockdown cells were slightly reduced by either SU5416 or Wortmannin (Supplementary Fig. 8a). SU5416 inhibited flow-directed upstream migration of control cells as well as downstream displacement of sh*ENG* ECs, indicating the requirement for VEGFR2 signalling in EC migration. Interestingly Wortmannin did not alter upstream migration of control ECs but inhibited downstream migration of sh*ENG* ECs (Supplementary Fig. 8b).

In conclusion, we demonstrate that *ENG* knockdown has no effect on VEGFR2 activation, but alters VEGFA-induced VEGFR2 kinetics. This likely contributes to the observed

enhanced AKT phosphorylation in the absence of ENG and may consequently feed into the development of AVMs in vivo. In accordance, drug mediated blockage of VEGFR2 or AKT in *Eng* LOF mice reduced AVM severity.

Discussion

ENG or *ALK1* LOF mutations lead to faulty regulation of processes normally involved in angiogenesis and vascular homeostasis and play a central role in the formation of AVMs. However, the sequence of events during the formation, and the origin of the malformation are incompletely resolved.

Here we show that *Eng* LOF cells are unable to follow instructive migratory cues provided by the direction of blood flow, in turn leading to local accumulation of *Eng* LOF cells and consequential AVM, expanding from arterioles (summarised in Fig. 8d). Furthermore, *Eng* LOF alters VEGFR2 kinetics and promotes downstream AKT signalling in response to VEGFA stimulation, providing mechanistic understanding of reduced AVM expansion following VEGFR2 inhibition. In agreement with previous studies34, 35 we demonstrate the effectiveness of either VEGFR2 or PI3K/AKT inhibition, here in *Eng* LOF mice, strengthening the hypothesis for the coupling of VEGFA/VEGFR2 signalling to the formation of AVM in HHT.

Although ENG and ALK1 are intimately connected our data suggest an opposing effect of ENG, to that reported for ALK1 on tip/stalk cell selection. Whereas *Eng* LOF results in reduced tip cell potential, *Alk1* LOF provides a cell autonomous tip cell advantage, and hypersprouting phenotype16, 25. This indicates that ENG is not required for tip-cell selection *per se*. *ENG* OE on the other hand leads to a strong over representation of *ENG* OE cells in the tip cell position, suggesting that ENG augments the ability to take, or maintain, the tip cell position. Despite the impact of ENG on tip cell capacity, neither *Eng* LOF nor OE strongly affected the overall sprouting. Only when *Eng* LOF causes large AVMs and hypoxia, hypersprouting is observed16. Together, these data show that tip-stalk selection is not directly related to initiation of AVMs in HHT.

Several studies have illustrated that ECs migrate against flow, but the importance of this in vascular patterning has not been exposed2, 26, 29–32. Here we show that ENG controls flow-directed migration in a dose-dependent manner, and is required for correct vascular morphogenesis. The strong selective enrichment of *Eng* LOF ECs in veins and *ENG* OE ECs in main arteries uncovers ENG as a potent regulator of artery-vein specification. Analysis of mosaic *Eng* LOF retinal vasculature reveals that AVMs predominantly arise from arterioles. This, together with strong *Eng* expression in arterioles of adult mice, highlights ENG's importance in these specific regions. During development the formation of arterioles involves a thinning of the previous immature structure, and dependent on anatomical location, display fewer ECs per length36. The lack of EC apoptosis during this period of development suggests that cell exclusion normally occurs by migration32. Hence, the sporadic accumulation of *Eng* LOF cells within expanding arterioles infers a locally reduced ability of ECs to escape the remodelling arterial structure by flow-mediated directional migration. Instead the retention of *Eng* LOF cells causes vessel expansion and AVM

development. This notion is strengthened by previous transcriptional and gene-ontology analyses of isolated ECs from HHT1 patients that imply reduced angiogenesis and EC migration37. To what extent the ENG-dependent flow-induced cellular behaviour relies on the ENG-mediated increase in flow sensitivity to BMP-mediated SMAD phosphorylation remains unknown38. Interestingly AVM establishment in *Alk1*-deficient zebrafish was shown to require flow and suggested to involve aberrant migratory behaviour36, 39.

Our data demonstrate ENG-mediated regulation of VEGFR2 signalling, providing potential mechanistic understanding of AVM development in *Eng* LOF and in HHT1 patients. We show ENG and VEGFR2 co-localisation in intracellular vesicles, and an effect of ENG on VEGFR2 kinetics after VEGFA stimulation, likely causing augmented AKT activation.

Modulating intracellular trafficking and recycling of VEGFR2, has been demonstrated to affect the balance between proliferation and migration, in response to VEGFA stimulation, thereby presenting similarities to signalling and behaviour of the *Eng* LOF ECs40. Although this exemplifies the power of alternative VEGFR2 trafficking to favour proliferation or migration, the determining mechanisms remain elusive. We observed that the AVM phenotype in ENG LOF postnatal retinas was relieved by inhibition of VEGFR2 or AKT. Similar results in *Alk1* LOF mice, indicate that AKT activity plays an important role in AVM also in HHT-234. Interestingly *Alk1* deletion causes also *Eng* downregulation, adding to the complexity of mechanistic contributions of *Alk1* and *Eng* in HHT15. Furthermore previous studies demonstrated that AKT phosphorylation promotes venous differentiation at the expense of arteriogenesis, an observation that supports our findings in HHT-141.

Vascular malformations are diverse in both aetiology and manifestation, and compose a large clinical problem. The cellular mechanisms underlying the formation of AVM in HHT1, such as misguided migration as described here, may also apply to other hereditary or sporadic vascular diseases. We demonstrate direct connections between ENG and VEGFR2 biology, providing an exciting basis for drug targeting of the VEGFA/VEGFR2/AKT signalling system in HHT1.

Supplementary Material

Refer to Web version on PubMed Central for supplementary material.

Acknowledgements

We thank Ralf Adams for providing the *Cdh5(PAC)-CreER*^{T2} mice, Calvin Vary for the *ENG*^{iOE} mice, Gavin Thurston (Regeneron) for providing the *Eng*^{LacZ} mice, Barbara Lavina and Konstantin Gaengel for sharing mice. We are grateful to Yan Xiong for help on the construction and package of lentivirus and to Annika Keller, Maarja Andaloussi Mäe and Kristian Pietras for initial contributions. This study was supported by grants from William K. Bowes Jr. Foundation (LJ), the Swedish Research Council (LJ, CB), the Swedish Cancer Society (LJ, CB), the Cardiovascular Programme and the Strategic Research Programme in Neuroscience at Karolinska Institutet (LJ), Jeanssons Stiftelser (LJ), Magnus Bergvalls Stiftelse (LJ), Knut and Alice Wallenbergs Stiftelse (CB), the European Research Council (CB), the Leducq Foundation (CB), the British Heart Foundation (HMA; RG/12/2/29416).

References

1. Herbert SP, Stainier DY. Molecular control of endothelial cell behaviour during blood vessel morphogenesis. Nat Rev Mol Cell Biol. 2011; 12:551–564. [PubMed: 21860391]

2. Udan RS, Vadakkan TJ, Dickinson ME. Dynamic responses of endothelial cells to changes in blood flow during vascular remodeling of the mouse yolk sac. Development. 2013; 140:4041–4050. [PubMed: 24004946]

3. Olsson AK, Dimberg A, Kreuger J, Claesson-Welsh L. VEGF receptor signalling - in control of vascular function. Nat Rev Mol Cell Biol. 2006; 7:359–371. [PubMed: 16633338]

4. Hellstrom M, et al. Dll4 signalling through Notch1 regulates formation of tip cells during angiogenesis. Nature. 2007

5. Leslie JD, et al. Endothelial signalling by the Notch ligand Delta-like 4 restricts angiogenesis. Development. 2007; 134:839–844. [PubMed: 17251261]

6. Lobov IB, et al. Delta-like ligand 4 (Dll4) is induced by VEGF as a negative regulator of angiogenic sprouting. Proc Natl Acad Sci U S A. 2007; 104:3219–3224. [PubMed: 17296940]

7. Siekmann AF, Lawson ND. Notch signalling limits angiogenic cell behaviour in developing zebrafish arteries. Nature. 2007

8. Harrington LS, et al. Regulation of multiple angiogenic pathways by Dll4 and Notch in human umbilical vein endothelial cells. Microvascular research. 2008; 75:144–154. [PubMed: 17692341]

9. Nakayama M, et al. Spatial regulation of VEGF receptor endocytosis in angiogenesis. Nature cell biology. 2013; 15:249–260. [PubMed: 23354168]

10. Krebs LT, et al. Haploinsufficient lethality and formation of arteriovenous malformations in Notch pathway mutants. Genes Dev. 2004; 18:2469–2473. [PubMed: 15466160]

11. Krebs LT, Starling C, Chervonsky AV, Gridley T. Notch1 activation in mice causes arteriovenous malformations phenocopied by ephrinB2 and EphB4 mutants. Genesis. 2010; 48:146–150. [PubMed: 20101599]

12. Nielsen CM, et al. Deletion of Rbpj from postnatal endothelium leads to abnormal arteriovenous shunting in mice. Development. 2014; 141:3782–3792. [PubMed: 25209249]

13. Murphy PA, et al. Constitutively active Notch4 receptor elicits brain arteriovenous malformations through enlargement of capillary-like vessels. Proc Natl Acad Sci U S A. 2014; 111:18007–18012. [PubMed: 25468970]

14. Mahmoud M, et al. Pathogenesis of arteriovenous malformations in the absence of endoglin. Circulation Research. 2010; 106:1425–1433. [PubMed: 20224041]

15. Tual-Chalot S, et al. Endothelial depletion of Acvrl1 in mice leads to arteriovenous malformations associated with reduced endoglin expression. PLoS One. 2014; 9:e98646. [PubMed: 24896812]

16. Aspalter IM, et al. Alk1 and Alk5 inhibition by Nrp1 controls vascular sprouting downstream of Notch. Nature communications. 2015; 6:7264.

17. Lebrin F, et al. Endoglin promotes endothelial cell proliferation and TGF-beta/ALK1 signal transduction. The EMBO journal. 2004; 23:4018–4028. [PubMed: 15385967]

18. Moya IM, et al. Stalk cell phenotype depends on integration of Notch and Smad1/5 signaling cascades. Developmental cell. 2012; 22:501–514. [PubMed: 22364862]

19. Choi EJ, et al. Novel brain arteriovenous malformation mouse models for type 1 hereditary hemorrhagic telangiectasia. PLoS One. 2014; 9:e88511. [PubMed: 24520391]

20. Choi EJ, et al. Minimal homozygous endothelial deletion of Eng with VEGF stimulation is sufficient to cause cerebrovascular dysplasia in the adult mouse. Cerebrovascular diseases. 2012; 33:540–547. [PubMed: 22571958]

21. Tual-Chalot S, Oh SP, Arthur HM. Mouse models of hereditary hemorrhagic telangiectasia: recent advances and future challenges. Frontiers in genetics. 2015; 6:25. [PubMed: 25741358]

22. Garrido-Martin EM, et al. Common and distinctive pathogenetic features of arteriovenous malformations in hereditary hemorrhagic telangiectasia 1 and hereditary hemorrhagic telangiectasia 2 animal models--brief report. Arterioscler Thromb Vasc Biol. 2014; 34:2232–2236. [PubMed: 25082229]

23. Blatt J, McLean TW, Castellino SM, Burkhart CN. A review of contemporary options for medical management of hemangiomas, other vascular tumors, and vascular malformations. Pharmacology & therapeutics. 2013; 139:327–333. [PubMed: 23665062]

24. Dupuis-Girod S, et al. Bevacizumab in patients with hereditary hemorrhagic telangiectasia and severe hepatic vascular malformations and high cardiac output. JAMA : the journal of the American Medical Association. 2012; 307:948–955. [PubMed: 22396517]
25. Larrivée B, et al. ALK1 signaling inhibits angiogenesis by cooperating with the Notch pathway. Developmental cell. 2012; 22:489–500. [PubMed: 22421041]
26. Jakobsson L, et al. Endothelial cells dynamically compete for the tip cell position during angiogenic sprouting. Nat Cell Biol. 2010; 12:943–953. [PubMed: 20871601]
27. Mancini ML, et al. Endoglin is required for myogenic differentiation potential of neural crest stem cells. Developmental Biology. 2007; 308:520–533. [PubMed: 17628518]
28. Arima S, et al. Angiogenic morphogenesis driven by dynamic and heterogeneous collective endothelial cell movement. Development. 2011; 138:4763–4776. [PubMed: 21965612]
29. Bussmann J, Wolfe SA, Siekmann AF. Arterial-venous network formation during brain vascularization involves hemodynamic regulation of chemokine signaling. Development. 2011; 138:1717–1726. [PubMed: 21429983]
30. Xu C, et al. Arteries are formed by vein-derived endothelial tip cells. Nature communications. 2014; 5:5758.
31. Ostrowski MA, et al. Microvascular endothelial cells migrate upstream and align against the shear stress field created by impinging flow. Biophysical journal. 2014; 106:366–374. [PubMed: 24461011]
32. Franco CA, et al. Dynamic endothelial cell rearrangements drive developmental vessel regression. PLoS Biol. 2015; 13:e1002125. [PubMed: 25884288]
33. Liu Z, et al. ENDOGLIN is dispensable for vasculogenesis, but required for vascular endothelial growth factor-induced angiogenesis. PLoS One. 2014; 9:e86273. [PubMed: 24489709]
34. Ola R, et al. PI3 kinase inhibition improves vascular malformations in mouse models of hereditary haemorrhagic telangiectasia. Nature communications. 2016; 7:13650.
35. Castillo SD, et al. Somatic activating mutations in Pik3ca cause sporadic venous malformations in mice and humans. Science translational medicine. 2016; 8:332ra343.
36. Rochon ER, Menon PG, Roman BL. Alk1 controls arterial endothelial cell migration in lumenized vessels. Development. 2016; 143:2593–2602. [PubMed: 27287800]
37. Fernandez LA, et al. Gene expression fingerprinting for human hereditary hemorrhagic telangiectasia. Hum Mol Genet. 2007; 16:1515–1533. [PubMed: 17420163]
38. Baeyens N, et al. Defective fluid shear stress mechanotransduction mediates hereditary hemorrhagic telangiectasia. J Cell Biol. 2016; 214:807–816. [PubMed: 27646277]
39. Corti P, et al. Interaction between alk1 and blood flow in the development of arteriovenous malformations. Development. 2011; 138:1573–1582. [PubMed: 21389051]
40. Jopling HM, et al. Endosome-to-Plasma Membrane Recycling of VEGFR2 Receptor Tyrosine Kinase Regulates Endothelial Function and Blood Vessel Formation. Cells. 2014; 3:363–385. [PubMed: 24785348]
41. Hong CC, Peterson QP, Hong JY, Peterson RT. Artery/vein specification is governed by opposing phosphatidylinositol-3 kinase and MAP kinase/ERK signaling. Curr Biol. 2006; 16:1366–1372. [PubMed: 16824925]

Europe PMC Funders Author Manuscripts

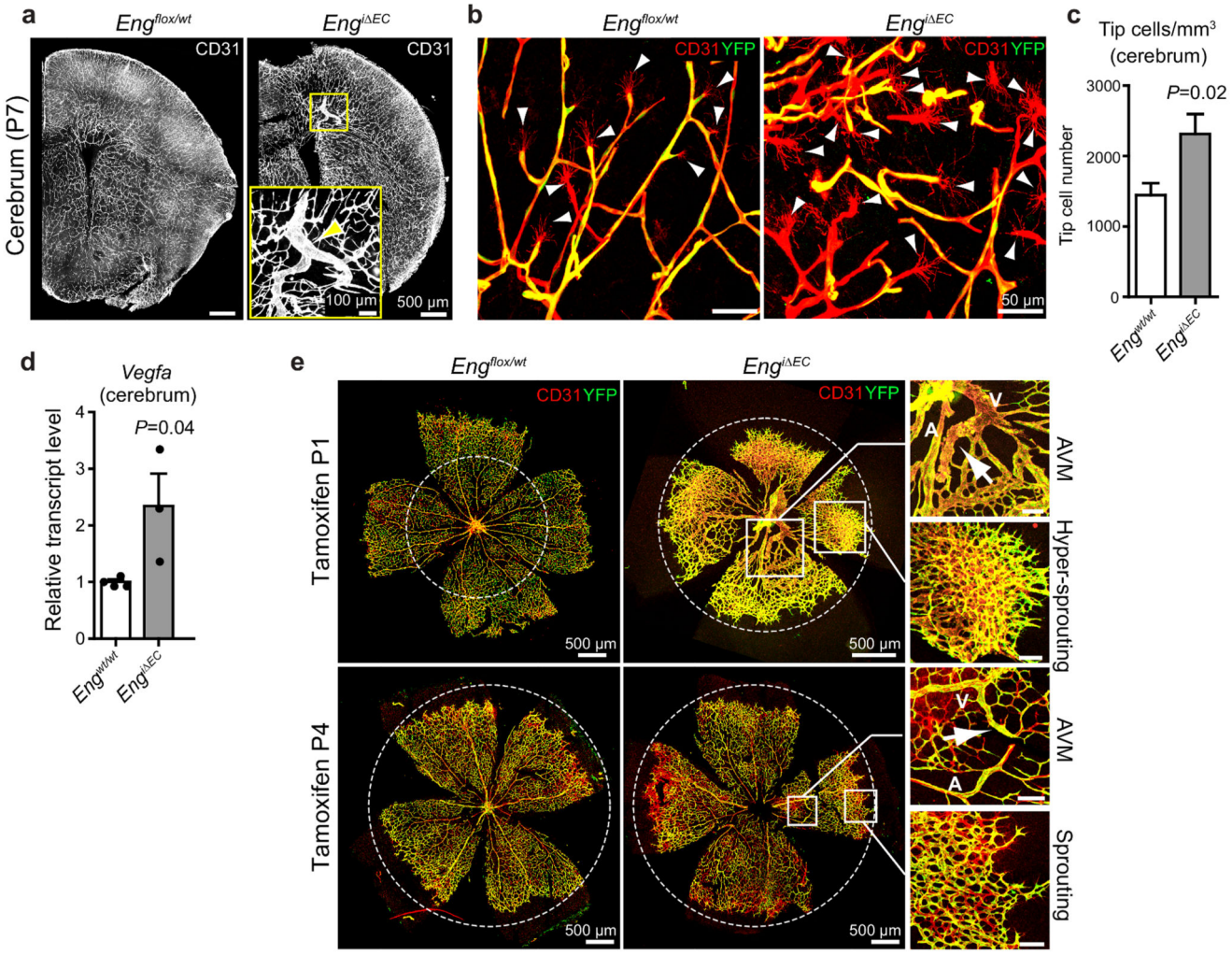

Figure 1. Postnatal EC-specific *Eng* LOF causes local AVM and secondary sprouting.

(**a**) The vasculature (CD31, white) within coronal sections of developing brains of control (*Eng*$^{flox/wt}$, left) and tamoxifen induced *Eng* LOF (induced P1, *Eng*$^{i\Delta EC}$, right) P7 mice. The boxed, zoomed area indicates an AVM following *Eng* LOF (arrow). Images are representative of five brains analysed for each genotype. Scale bars, 500μm (whole pictures); 100μm (Boxed area). (**b**) Cortical vasculature of P7 control mice (left) and *Eng* LOF (right) mice indicating increased tip cell formation. Arrowheads indicate filopodia-rich tip cells. ECs were stained for CD31 (red) and recombination assessed by YFP expression (Yellow). Scale bars, 50μm. (**c**) Quantification of tip cell numbers of the cerebral vasculature of P7 mice. Ten images were quantified from each brain. *Eng*$^{wt/wt}$, n=8 mice; *Eng*$^{i\Delta EC}$, n=5 mice. *P*=0.02. (**d**) *Vegfa* mRNA levels measured by quantitative PCR from total brain lysates of P7 mice. *Eng*$^{wt/wt}$, n=4 mice; *Eng*$^{i\Delta EC}$, n=3 mice *P*=0.04. Values are mean ± S.E.M. Significances in (**c, d**) were determined by two-tailed unpaired *t*-test. Statistics source data are shown in Supplementary Table 1. (**e**) The developing retinal vasculature of P7 *Eng*$^{flox/wt}$ (left) and *Eng*$^{i\Delta EC}$ (right) mice displaying radial expansion (dotted circles), AVMs (boxed) and sprouting front (boxed) within the same retinas following long term or short term *Eng*

Europe PMC Funders Author Manuscripts

LOF. Gene deletion was induced by tamoxifen injection at P1 (upper panel) or P4 (lower panel). Note the different scale in control versus *Eng* LOF. The dotted circles are of the same absolute size for comparison. A: artery; V: vein. Images are representative of at least 8 retinas analysed. Scale bars, 500μm (whole pictures); 100μm (boxed areas).

Europe PMC Funders Author Manuscripts

Europe PMC Funders Author Manuscripts

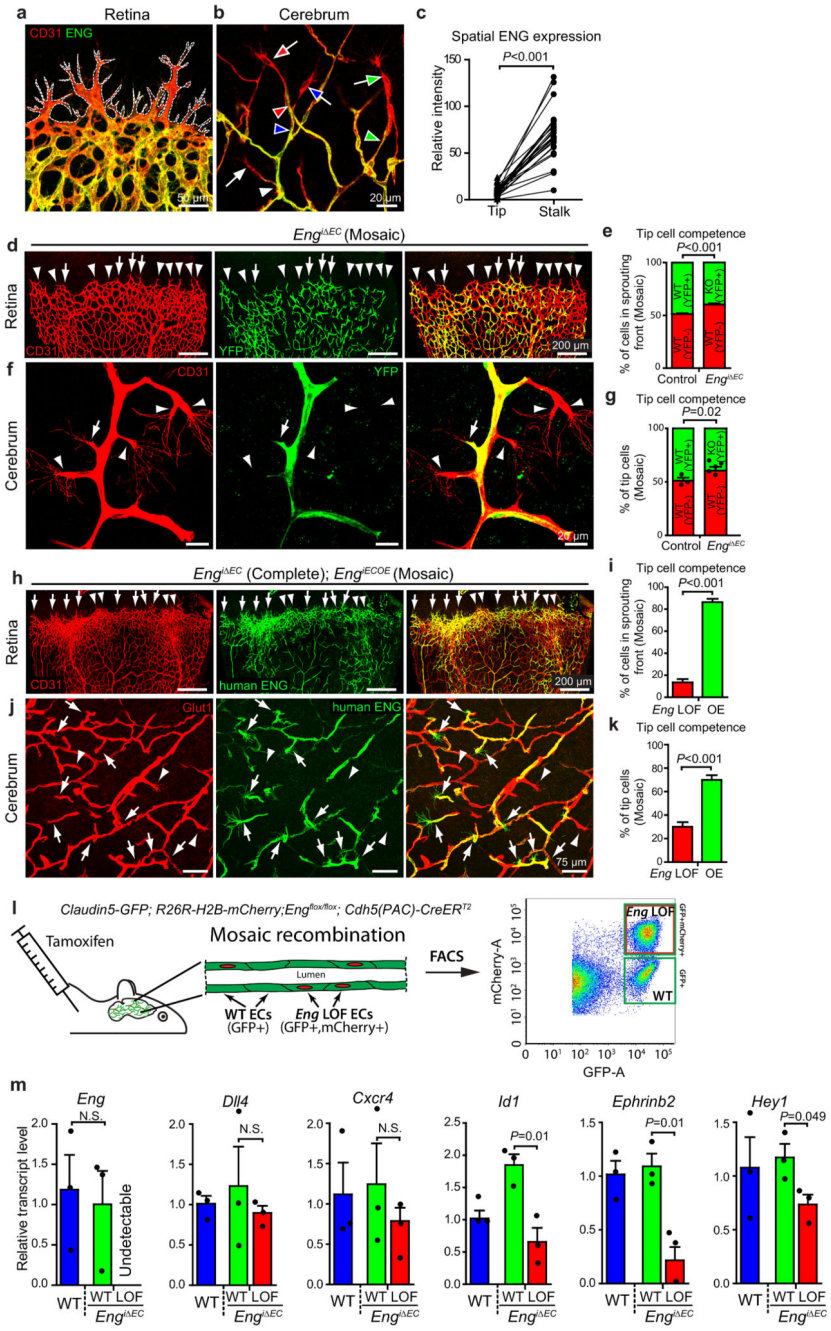

Figure 2. *Eng* expression is suppressed in tip- versus stalk- cells, but promotes tip cell potential.

(**a**) Retinas from P7 WT mice, stained for ECs (CD31) and for ENG. Dotted white line outlines the sprouting front. Images are representative of 8 retinas analysed. Scale bar, 50μm. (**b**) Brain vasculature of WT mice at P7, stained for ECs (CD31) and for ENG. Tip cells and their corresponding stalk cells are indicated by colour-coded arrows and arrowheads respectively. Scale bar, 20μm. (**c**) Quantification of fluorescent intensities of ENG-Immunolabelled brain tip cells and corresponding stalk cells (pairwise connected by lines), n=25 tip and stalk cells each from 5 WT brains. $P<0.001$. (**d, f, h, j**) The retinal or

brain vasculature of P7 *Eng*$^{i\Delta EC}$ and *Eng*$^{i\Delta EC+iOE}$ mice with mosaic recombination. CD31 or GLUT1 immunostaining indicates all ECs. (**d, f**) *Eng* LOF cells are identified by the YFP reporter (arrows) and non-recombined WT cells by CD31 only (arrowheads). Scale bars, 200μm (**d**); 20μm (**f**). (**h, j**) ECs with the human ENG transgene were stained for human ENG . *ENG* OE ECs (arrows) or *Eng* LOF ECs (arrowheads) in the sprouting front. Scale bars, 200μm (**h**); 75μm (**j**). (**e, g**) Quantification of tip cell competences of recombined (YFP +) or non-recombined (YFP-) ECs within the retinal (**e**) or brain (**g**) vasculature of P7 WT or mosaic *Eng* LOF mice. (**e**) Control, n=5 retinas; *Eng*$^{i\Delta EC}$, n=9 retinas. $P<0.001$. (**g**) Control, n=3 mice; *Eng*$^{i\Delta EC}$, n=5 mice. $P=0.02$. (**i, k**) Quantifications of tip cell competence of LOF or OE (human ENG+) cells within the P7 retinas or cerebral vasculature of *Eng*$^{i\Delta EC+iOE}$ mice. (**i**) n=15 retinas. $P<0.001$. (**k**) n=19 cerebral areas from 6 mice. $P<0.001$.(**l**) Schematic pictures describing the FACS sorting of the *Eng* LOF and WT EC populations from the cerebral vasculature of the same mouse by the use of Claudin5-GFP and R26R-H2B-mCherry reporters. (**m**) Changes of gene-expression following *Eng* deletion were assessed by q-PCR from *Eng* LOF ECs compared with *Eng* WT ECs isolated by FACS from *Eng*$^{i\Delta EC}$ brains of P8-9 mice, n=3 mice each for *Eng* WT and *Eng*$^{i\Delta EC}$. $P=0.01$ (*Id1*); $P=0.01$ (*Ephrinb2*); $P=0.049$ (*Hey1*), between *Eng* WT and LOF cells in *Eng*$^{i\Delta EC}$ mice. All values are mean ± S.E.M. Significances in (c, e, g, i, k, m) were determined by two-tailed unpaired *t*-test. Statistics source data are shown in Supplementary Table 1.

Europe PMC Funders Author Manuscripts

Europe PMC Funders Author Manuscripts

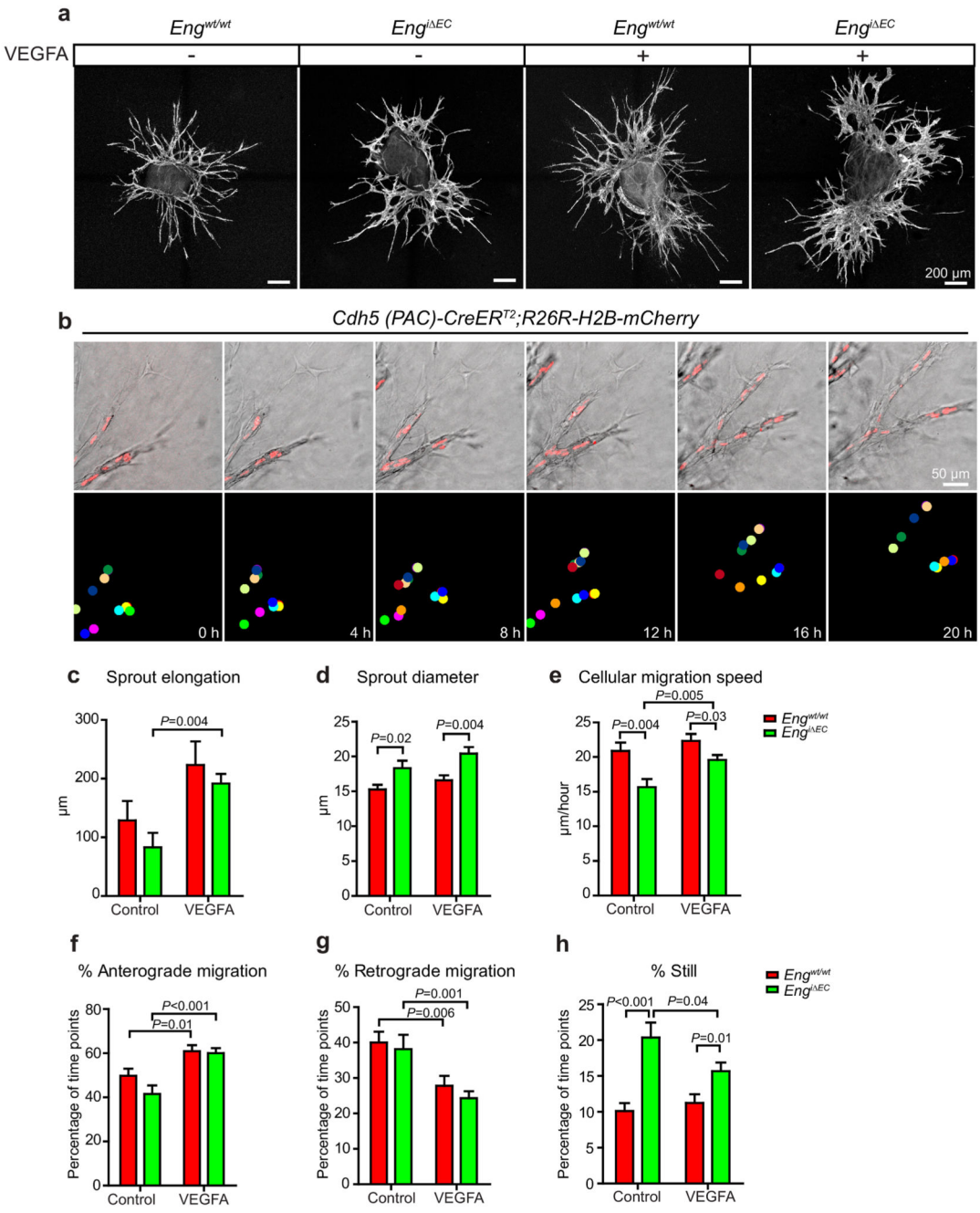

Figure 3. *Eng* LOF reduces EC migration in sprouting angiogenesis

(**a**) Representative overview images of EC sprouts (CD31, white) from aortic ring explants cultured in medium with indicated treatments for 48 hours. Scale bars, 200µm. (**b**) Snapshots from a time-lapse sequence of growing sprouts of an aortic ring with induced nuclear-localized mCherry under the EC-specific Cdh5 promoter (upper panel). Nuclei of individual cells were labelled with colour coded dots for tracking and quantification in ImageJ (lower panel). Scale bar, 50µm. (**c**) Quantification of the elongation of sprouts during the first 24 hours of treatment. WT control, n=9 sprouts from 3 aortic rings; WT VEGF, n=7

Europe PMC Funders Author Manuscripts

sprouts from 4 aortic rings; $Eng^{i\Delta EC}$ control, n=9 sprouts from 3 aortic rings; $Eng^{i\Delta EC}$ VEGF, n=7 sprouts from 4 aortic rings. P=0.004 between $Eng^{i\Delta EC}$ control and $Eng^{i\Delta EC}$ VEGFA. (**d**) Quantifications of the diameters of the vascular sprouts on fixed samples. n=45 sprouts from 8-10 rings for each condition. Control, P=0.02; VEGFA, P=0.04, between WT and $Eng^{i\Delta EC}$. (**e-h**) Quantifications of cell migration speed and directions during the sprouting process under different conditions reveals reduced migration of *Eng* LOF ECs (see more details in Methods). WT control, n=22 live imaged cells from 3 aortic rings; WT VEGF, n=26 cells from 4 aortic rings; $Eng^{i\Delta EC}$ control, n=18 cells from 3 aortic rings; $Eng^{i\Delta EC}$ VEGF, n=38 cells from 4 aortic rings. (**e**) Control, P=0.004; VEGFA, P=0.03, between WT and $Eng^{i\Delta EC}$. P=0.005 between $Eng^{i\Delta EC}$ control and $Eng^{i\Delta EC}$ VEGFA. (**f**) WT, P=0.01; $Eng^{i\Delta EC}$, P<0.001, between control and VEGFA treated samples. (**g**) WT, P=0.006; $Eng^{i\Delta EC}$, P=0.001, between control and VEGFA treated samples. (**h**) Control, P<0.001; VEGFA, P=0.01, between WT and $Eng^{i\Delta EC}$. P=0.04 between $Eng^{i\Delta EC}$ control and $Eng^{i\Delta EC}$ VEGFA. Data are pooled from 2 independent experiments and represent mean ± S.E.M. Significances in (c-h) were determined by two-tailed unpaired *t*-test.

Europe PMC Funders Author Manuscripts

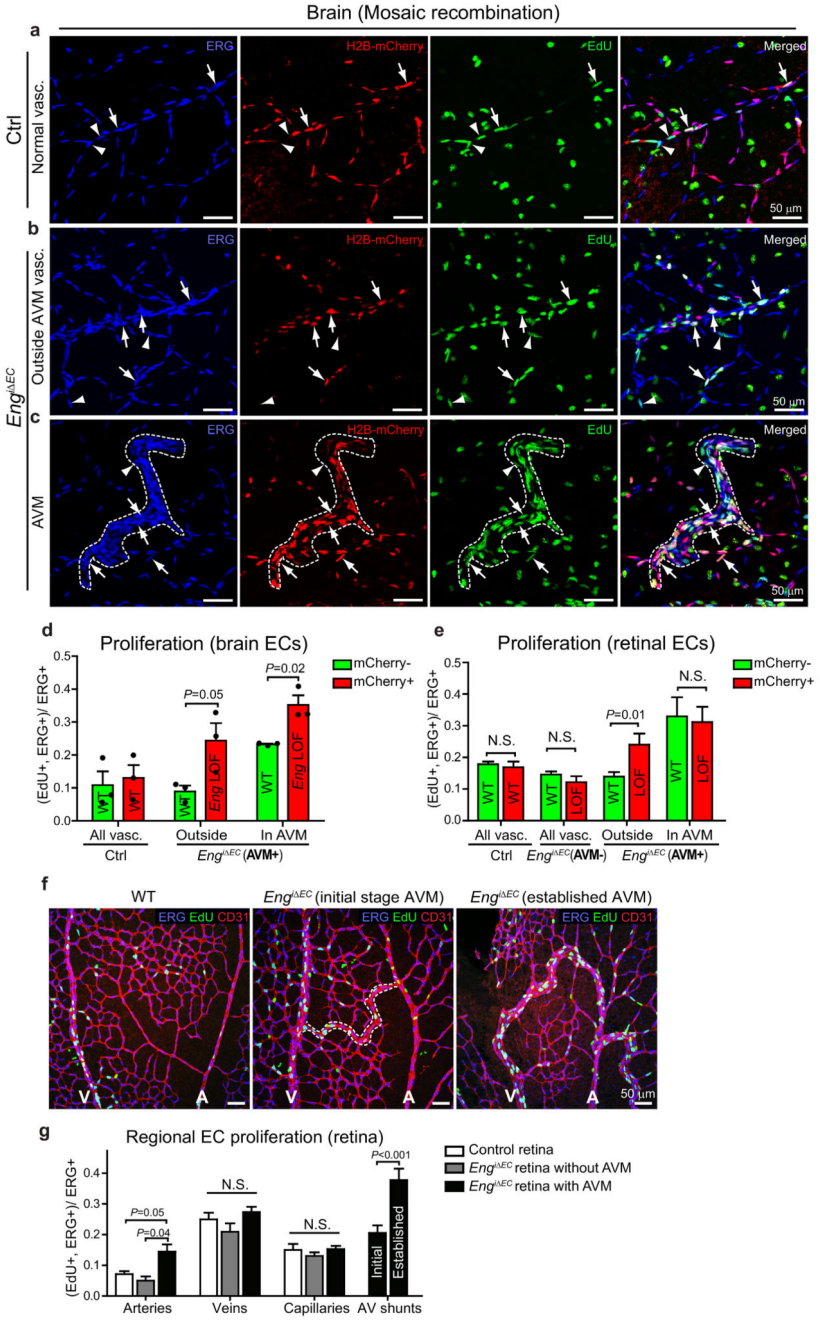

Figure 4. *Eng* LOF mediates context-dependent effects on proliferation.

(**a-c**) Cerebral vessels of P7 mice carrying a conditional nuclear-localized mCherry under an EC-specific promoter, allowing for identification of recombined ECs (H2B-mCherry, red). Arrowheads indicate proliferating non-recombined ECs (mCherry-, EdU+, ERG+) and arrows indicate proliferating recombined ECs (mCherry+, EdU+, ERG+). Right most panels are overlays of the ones to the left. (**a**) Normal vasculature of control mice with mosaic mCherry recombination. (**b**) Morphologically normal vasculature of *Eng*$^{i\Delta EC}$ mice displaying mosaic recombination. (**c**) AVM-like structure (outlined by dotted line) of

Eng$^{i\Delta EC}$ mice. (**d**) Quantification of percentage of proliferating recombined and non-recombined ECs out of total ECs in cerebral vessels. Three to five different regions (covering either malformations or normal areas) were counted and summed as one brain for quantification (n=3 mice each for WT and *Eng*$^{i\Delta EC}$). P=0.05 (“outside”); P=0.02 (“in AVM”), between *Eng* WT and LOF cells. Statistics source data are shown in Supplementary Table 1. (**e**) Quantification of percentage of proliferating recombined and non-recombined ECs out of total ECs in retinal vessels. WT, n=9 retinas; AVM-, n=9 retinas; AVM+, n=12 retinas; AVM regions, n=13 AVMs. P=0.01 (“outside”) between *Eng* WT and LOF cells. (**f**) Proliferating ECs in P7 retinas were shown by co-staining for EdU (green), ERG (blue) and CD31. (**g**) Quantification of proliferation of ECs in the arteries, veins, capillaries and AV shunts in retinas. Arteries, control, n=12 vessels; *Eng*$^{i\Delta EC}$ without AVM, n=8 vessels; *Eng*$^{i\Delta EC}$ with AVM, n= 29 vessels. Veins, control, n=12 vessels; *Eng*$^{i\Delta EC}$ without AVM, n=5 vessels; *Eng*$^{i\Delta EC}$ with AVM, n= 23 vessels. Capillaries, control, n=12 areas; *Eng*$^{i\Delta EC}$ without AVM, n=14 areas; *Eng*$^{i\Delta EC}$ with AVM, n= 24 areas. Initial AV shunts, n=23 vessels. Established AV shunts, n=15 vessels. P=0.05 between arteries in control and *Eng*$^{i\Delta EC}$ with AVM. P=0.04 between arteries in *Eng*$^{i\Delta EC}$ without AVM and *Eng*$^{i\Delta EC}$ with AVM. P<0.01 between initial and established AV shunts. Significances in (d, e, g) were determined by two-tailed unpaired t-test. All values are mean ± S.E.M. N.S.= not significant. Scale bars, 50μm.

Europe PMC Funders Author Manuscripts

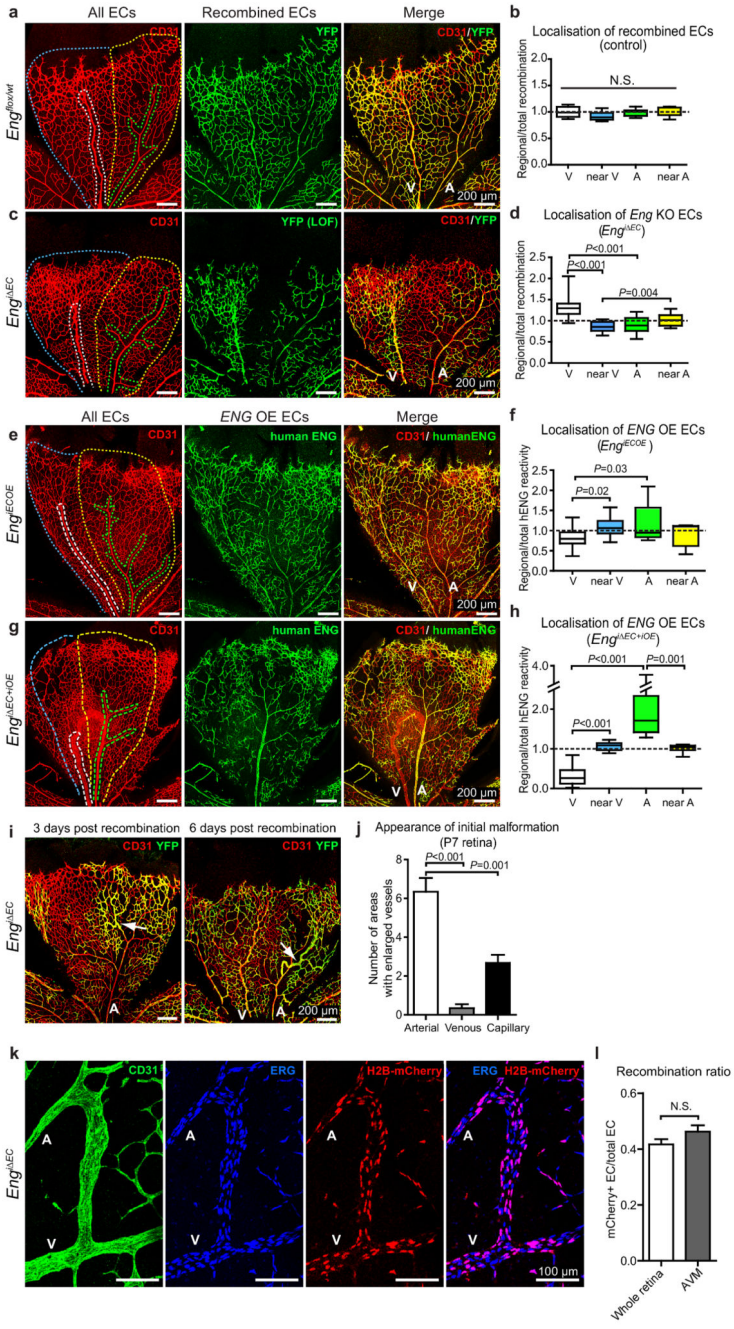

Figure 5. Loss- or gain- of ENG alters retinal EC distribution and *Eng* deletion initiates AVM in arterioles.

(**a**, **c, e, g**) P7 retinal vasculature of $Eng^{flox/wt}$:*Cdh5(PAC)CreER*^{T2}:*R26Ryfp* ($Eng^{flox/wt}$), $Eng^{i\Delta EC}$, Eng^{iECOE} and $Eng^{i\Delta EC+iOE}$ pups induced with tamoxifen. Vessels were stained for CD31 (red) to indicate all ECs and for YFP to visualize tamoxifen-induced control ($Eng^{flox/wt}$) or LOF ECs (green in **a**, **c**). Human ENG were stained to visualize *ENG* OE cells (green in **e**, **g**). Scale bars, 200μm. (**b**, **d**) The ratio of regional/total recombination area (YFP+) was calculated for each retinal leaflet containing both an artery and a vein from

Europe PMC Funders Author Manuscripts

control (*Eng*$^{flox/wt}$) or *Eng*$^{i\Delta EC}$ respectively. *Eng*$^{flox/wt}$, n=8 retinal regions from 3 mice. *Eng*$^{i\Delta EC}$, n=13 retinal regions from 4 mice, $P<0.001$ between "V" and "A" or "near V"; $P=0.004$ between "near V" and "near A". (**f, h**) The ratio of regional/total percentage of ENG OE cells was calculated for each retinal leaflet containing both an artery and a vein from *Eng*^{iECOE} or *Eng*$^{i\Delta EC+iOE}$. *Eng*^{iECOE}, n=11 retinal regions from 5 mice, $P=0.03$ between "V" and "A"; $P=0.02$ between "V" and "near V". *Eng*$^{i\Delta EC+iOE}$, n=10 retinal regions from 4 mice, $P<0.001$ between "V" and "A" or "near V"; $P=0.001$ between "A" and "near A". Box plots display values of minimum, first quartile, median, third quartile, and maximum. Regions were segmented as indicated in (**a**), (**c**), (**e**) and (**g**) where white is venous (V), blue is near vein (near V), green is arterial (A) and yellow near artery (near A). Retinas with 20-80% total recombination were used for the quantification.; (**i**) Retinal vasculature of *Eng*$^{i\Delta EC}$ mice at P7, induced for mosaic recombination at either P4 (left) or P1 (right). Arrows indicate abnormal arterioles suggesting initiation of AVMs. Scale bars, 200μm. (**j**) Quantification of anatomical localization of malformation initiation in P7 retinas following mosaic recombination at P4, n=6 retinas. $P<0.001$ between arterial and venous regions; $P=0.001$ between arterial and capillary regions. Data represent mean ± S.E.M. (**k**) An AVM in a mosaic recombined *Eng* LOF retina. ECs are stained with CD31 (green) and ERG (blue) antibody. Nuclear localized H2B-mCherry (red) shows ECs with recombination. Scale bars, 100μm. (**l**) Quantification of recombination ratio of AVMs in the mosaic recombined retinas, compared with the recombination ratio of the whole retinas. 17 AVMs in 5 retinas were quantified. A: artery; V: vein. All values are mean ± S.E.M. Significances in (b, d, f, h, j, l) were determined by two-tailed unpaired *t*-test. N.S.= not significant.

Europe PMC Funders Author Manuscripts

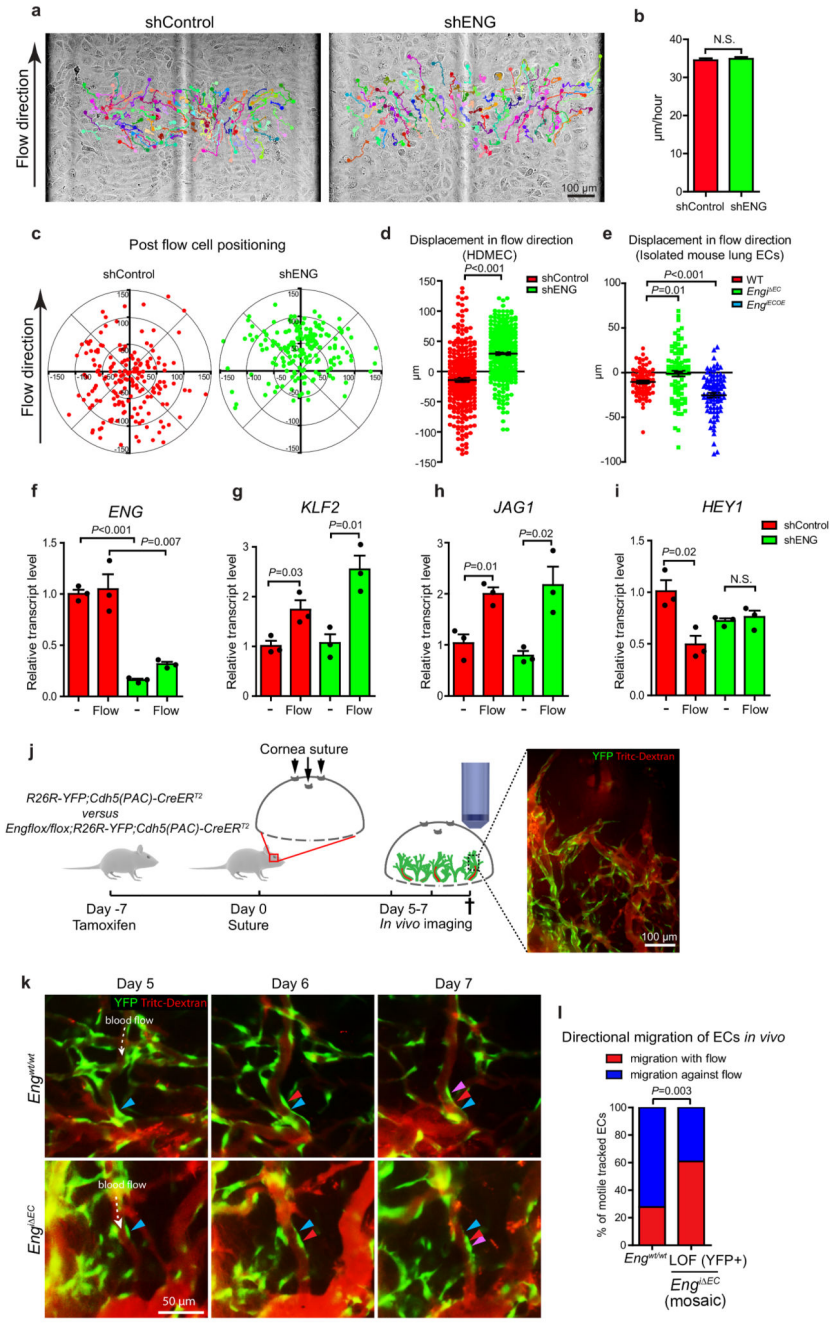

Figure 6. ENG regulates EC migration in response to shear stress and blood flow.

(**a**) Bright field images of HDMECs under laminar flow (7.5 dyne/cm^2) acquired every 5 minutes for 5 hours. Individual cell tracks and migratory routes are indicated by colours. Scale bar, 100μm. (**b**) Migration speed of control and ENG knockdown cells. Migration speed of individual cells was calculated as migration distance/time. Control, n=295 cells; sh*ENG*, n=287 cells (pooled from 3 experiments per condition) (**c**) Relative positions of the cells after being subjected to flow for 5 hours. Each dot represents an individual cell with original position set at (0,0). (**d**) The displacement of HDMECs migration towards direction

of flow (Y axis). Data derive from the same experiments as in (b). $P<0.001$, two-tailed unpaired *t*-test. (**e**) The displacement of isolated mouse lung ECs migration towards direction of flow (Y axis). WT, n=83 cells; $Eng^{i\Delta EC}$, n=89 cells; Eng^{iECOE}, n=95 cells (pooled from 2 independent experiments. $P=0.01$ between WT and $Eng^{i\Delta EC}$; $P<0.001$ between WT and Eng^{iECOE}, two-tailed unpaired *t*-test). (**f-i**) Relative transcript levels of *ENG*, *KLF2*, *JAG1*, *HEY1* in control and ENG knockdown cells with or without flow treatment are determined by qPCR. n=3 independent experiments. Statistics source data are shown in Supplementary Table 1. Significances were determined by two-tailed unpaired *t*-test. (**f**) $P<0.001$ (without flow); $P=0.007$ (Flow), between shControl and shENG. (**g**) $P=0.03$ (shControl); $P=0.01$ (shENG), between "-" and "Flow". (**h**) $P=0.01$ (shControl); $P=0.02$ (shENG), between "-" and "Flow". (**i**) $P=0.01$ (shControl) between "-" and "Flow". (**j**) Schematic pictures describing the timeline of the cornea suture model. Scale bar, 100μm. (**k**) Representative pictures showing directional migration of ECs in WT and $Eng^{i\Delta EC}$. Expression of YFP is switched on in subsets of ECs (green). Vessels are visualized by I.V. injection of Tritc-dextran (red). Direction of blood flow is indicated by white arrows. Positions of the cells at day 5, 6 and 7 are indicated by blue, red and purple arrowheads respectively. Scale bar, 50μm. (**l**) Quantification of percentages of ECs migrating with or against flow direction. *Eng* WT, n=36 tracked migrating ECs (pooled data from 3 mice); *Eng* LOF, n=46 tracked migrating ECs (pooled data from 4 mice).$P=0.003$, Chi-squared test. Error bars represent S.E.M. N.S.=not significant.

Europe PMC Funders Author Manuscripts

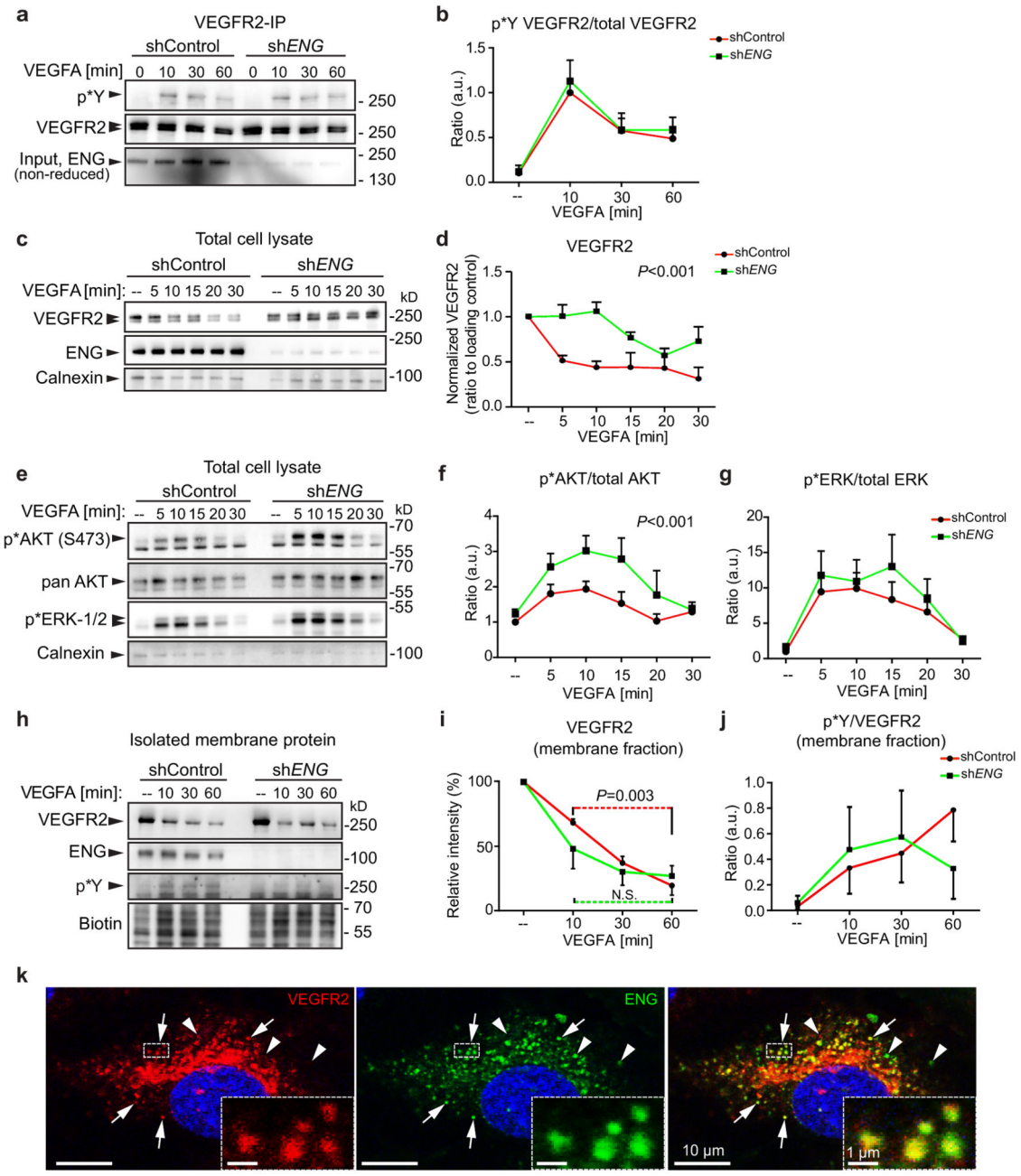

Figure 7. ENG affects VEGFR2 trafficking and downstream signalling.

(**a**) Immunoprecipitation of VEGFR2 with protein samples from VEGF-treated HDMECs lenti-virally transduced with either control shRNA or shRNA targeting *ENG.* Phosphorylated VEGFR2 was detected by blotting with pTyr antibody. (**b**) Ratio of Phosphorylated/total VEGFR2 was measured by ImageJ, n=4 independent experiments. (**c, d**) Western blot of total cell lysates of HDMECs, indicates knockdown of *ENG* in the sh*ENG* condition (non-reduced condition). VEGFA treatment for indicated time points reveals differential loss of VEGFR2 over time in control versus knockdown cells as shown

Europe PMC Funders Author Manuscripts

by densitometric analysis relative to the loading control calnexin. $P<0.001$, 2-way ANOVA, n=3 independent experiments. (**e**) Total cell lysates of the above analysed for VEGFR2 downstream components p*AKT, pan AKT, p*ERK1/2 and the loading control calnexin. (**f, g**) Densitometric quantification of p*AKT/total AKT or p*ERK1/2 /total ERK showing potentiated AKT phosphorylation in *ENG* knockdown ECs ($P<0.001$, 2-way ANOVA, n=7 independent experiments for time points 0, 10, 30 min; n=3 independent experiments for time points 5, 15, 20 min) and no difference in p* ERK1/2. (**h**) Cellular membrane proteins were isolated at different time points and analysed for VEGFR2 (note the absence of the intracellular unglycosylated band), ENG, p*Y and total amount (biotin). (**i**) Densitometric analysis of membrane localised VEGFR2 in (**h**). Red or green dotted line indicates comparison between 10 and 60 minutes for the control or shENG cells, respectively. n=3 independent experiments. $P=0.003$ (shControl) between 10 and 60 minutes, two-tailed unpaired *t*-test. (**j**) Phosphorylated VEGFR2 within the cell membrane was detected with anti-phospho-Tyrosine antibody (p*Y and ratios of phosphorylated/total VEGFR2 at different time points were plotted. n=3 independent experiments. No difference between shControl and shENG, 2-way ANOVA. (**k**) Co-staining for VEGFR2 (red) and ENG (green) in HDMECs treated with VEGF (50ng/ml) for 10 min. VEGFR2 and ENG colocalise in subsets of intracellular vesicles (indicated by arrows and the dashed line box). Arrowheads indicate non-colocalising VEGFR2 or ENG. Co-localisation of signals within the boxed region was analysed by Volocity. Images are representative of 3 independent experiments. Scale bars, 10μm (whole pictures); 1μm (boxed areas). Unprocessed scans of the blots shown in (**a, c, e, h**) are provided in supplementary figure 9. Statistics source data are shown in Supplementary Table 1. a.u. = Arbitrary units.

Europe PMC Funders Author Manuscripts

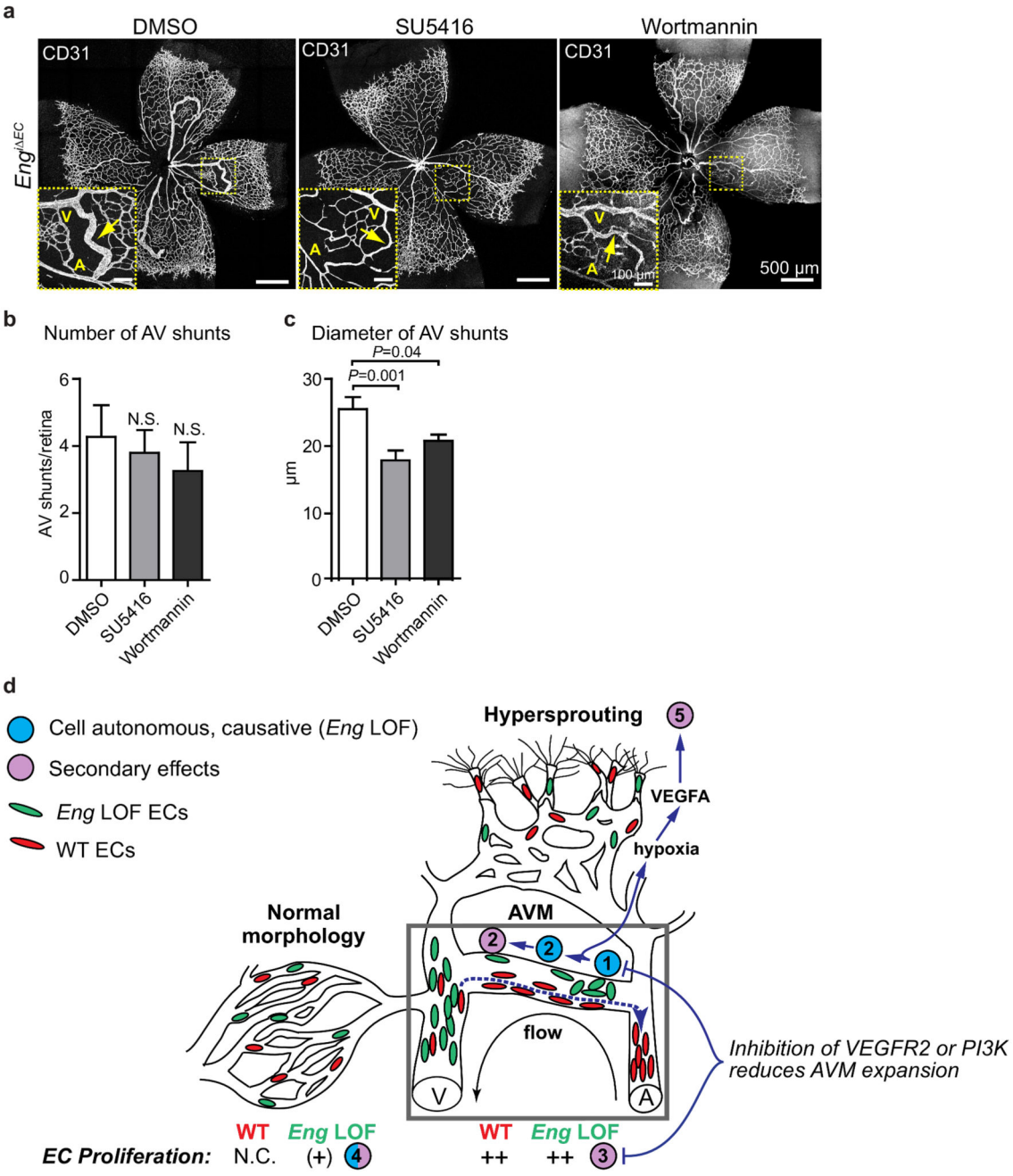

Figure 8. Effects of VEGFR2 or PI3K inhibition on AVM properties and summary of concepts.

(**a**) P7 retinas from $Eng^{i\Delta EC}$ mice (tamoxifen injected at P3) treated with SU5416 or Wortmannin at P4-6. Yellow boxes show regions with AVMs (inset). Arrows indicate AVMs. A: artery; V: vein. Scale bars, 500µm (whole pictures); 100µm (boxed areas). (**b, c**) Quantification of the numbers and the diameters of retinal AVMs from mice treated with DMSO, SU5416 or Wortmannin. (**b**) DMSO, n=11 retinas; SU5416, n=10 retinas; Wortmannin, n=8 retinas. (**c**) DMSO, n=41 AV shunts from 11 retinas; SU5416, n=41 AV shunts from 10 retinas; Wortmannin, n=27 AV shunts from 8 retinas. *P*=0.001 between

DMSO and SU5416; P=0.04 between DMSO and Wortmannin, two-tailed unpaired t-test. **(d) Schematic summary of findings.** *Eng* LOF disturbs normal allocation and specification of ECs in the developing vasculature by cell-autonomous reduction of flow-directed migration, which leads to initiation of AVM, followed by non-cell autonomous effects on proliferation that contribute to the expansion of the AVM. (**1**) Lack of flow-sensing by *Eng* LOF cells (green) prevents normal migration (red cells, blue dotted line) against flow into the main artery thereby leading to (**2**) clonal cohesion and enlargement of the vessel causing initiation (primary, cell autonomous) and expansion (secondary, non-cell autonomous) of AVM. (**3**) Highly proliferative ECs including both *Eng* WT and LOF cells are found in well-established AV shunts. (**4**) *Eng* LOF ECs display a cell-autonomous increase in proliferation in the vasculature adjacent to AVM. Proliferation is not affected in mosaic *Eng* LOF vasculature of retinas lacking AVM. (**5**) AVMs in turn cause insufficient oxygenation, driving VEGFA production that stimulates sprouting angiogenesis despite the reduced tip cell potency of *Eng* LOF ECs (green). *Eng* LOF alters VEGFR2 signalling with potentiated AKT phosphorylation. This may, at least in part, be the underlying cause of the disturbed migratory response, which could explain the protective effects of VEGFR2 inhibition on AVM. N.C., not changed.

Europe PMC Funders Author Manuscripts